

# Prediction of the As-Cast Structure of Al-4.0 Wt Pct Cu Ingots

MAHMOUD AHMADEIN, M. WU, J.H. LI, P. SCHUMACHER, and A. LUDWIG

A two-stage simulation strategy is proposed to predict the as-cast structure. During the first stage, a 3-phase model is used to simulate the mold-filling process by considering the nucleation, the initial growth of globular equiaxed crystals and the transport of the crystals. The three considered phases are the melt, air and globular equiaxed crystals. In the second stage, a 5-phase mixed columnar-equiaxed solidification model is used to simulate the formation of the as-cast structure including the distinct columnar and equiaxed zones, columnar-to-equiaxed transition, grain size distribution, macrosegregation, *etc.* The five considered phases are the extradendritic melt, the solid dendrite, the interdendritic melt inside the equiaxed grains, the solid dendrite, and the interdendritic melt inside the columnar grains. The extra- and interdendritic melts are treated as separate phases. In order to validate the above strategy, laboratory ingots (Al-4.0 wt pct Cu) are poured and analyzed, and a good agreement with the numerical predictions is achieved. The origin of the equiaxed crystals by the “big-bang” theory is verified to play a key role in the formation of the as-cast structure, especially for the castings poured at a low pouring temperature. A single-stage approach that only uses the 5-phase mixed columnar-equiaxed solidification model and ignores the mold filling can predict satisfactory results for a casting poured at high temperature, but it delivers false results for the casting poured at low temperature.

DOI: 10.1007/s11661-012-1606-6

© The Minerals, Metals & Materials Society and ASM International 2013

## I. INTRODUCTION

A good understanding of the solidification phenomena, such as the origin of equiaxed and columnar grains, the evolution of globular/cellular morphology to dendritic, and the columnar-to-equiaxed transition (CET), has been the focal issue among the researchers to develop models which are needed to predict the solidification structure. Despite the several empirical models introduced, no sufficient attention has been paid to incorporate them together with macroscopic phenomena. The as-cast structure has a crucial impact on the mechanical properties of cast products. For decades, researchers and metallurgists have been studying the factors which affect the as-cast structure.<sup>[1–5]</sup> Once the nucleation of equiaxed grains occurs (heterogeneously or under dynamically stimulated conditions), metal crystals start to grow in

either columnar (cellular or dendritic) or in equiaxed (globular or dendritic) morphology. The final as-cast structure may contain one or more of these morphologies with a CET. In addition, various interacting multiphase/multiscale processes during solidification, *e.g.*, transport of heat, momentum, mass, species, and melt convection increase the complexity of the prediction of the as-cast structure.

Progress has also been extended to grasp a better understanding of CET since the pioneer study of Hunt<sup>[6]</sup> in the 1980s. A CET map using a correlation of the columnar primary dendrite tip growth velocity with the local temperature gradient at the moment of CET was established to analyze the occurrence of CET. This CET map was later verified and further improved by many authors.<sup>[7–12]</sup> In the meantime, empirical correlations have been proposed as indirect criteria to predict the CET for engineering castings.<sup>[13–17]</sup>

In later studies,<sup>[18–21]</sup> Wu and co-authors introduced a 5-phase mixed columnar-equiaxed model which takes into account the impacts of flow and grain transport based on the above mentioned empirical knowledge. Preliminary simulations were compared with Al-Cu alloy ingots which are poured at various temperatures.<sup>[22,23]</sup> The results showed that the model is capable of producing the mixed columnar-equiaxed structure and to distinguish the CET, but fails to predict the fully equiaxed structure obtained at low pouring temperature.

The reason for the failure prediction of the as-cast structure for the castings poured at low pouring temperature consists in the fact that the mold filling and its influence on the origin of crystals were ignored.

---

MAHMOUD AHMADEIN, Post-Doctoral Researcher, is with the Chair for Modeling and Simulation of Metallurgical Processes, University of Leoben, Leoben, Austria and also Assistant Professor with the Production Engineering & Mechanical Design Department, Faculty of Engineering, Tanta University, Tanta, Gharbia, Egypt. Contact e-mail: mahmoud.ahmadein@unileoben.ac.at M. WU, Associate Professor, is with the Chair for Modeling and Simulation of Metallurgical Processes, University of Leoben and also with the Christian-Doppler Laboratory for Advanced Process Simulation of Solidification & Melting, University of Leoben, Leoben, Austria. J.H. LI, Research Assistant, and P. SCHUMACHER, Professor, are with the Chair for Casting Research, University of Leoben, Leoben, Austria. A. LUDWIG, Professor, is with the Chair for Modeling and Simulation of Metallurgical Processes, University of Leoben.

Manuscript submitted September 17, 2012.

Article published online January 24, 2013

Previous simulations were based on an assumption that same and constant initial number density of the equiaxed grains ( $n_0$ ) are applied despite the difference in the pouring temperature. According to the “big-bang”<sup>[2]</sup> or “separation” theory,<sup>[4]</sup> a large amount of equiaxed nuclei would be produced during pouring at the first contact of the melt with the cold mold. These nuclei would subsequently be dispersed in the bulk melt.

In the current study, further model verifications and improvements of the authors’ earlier studies<sup>[18–23]</sup> have been conducted. Mold filling, which had been ignored completely in previous studies, is now being considered to predict more reliable initial conditions that are required for the prediction of the as-cast structure and CET using the 5-phase columnar/equiaxed model. There was much experimental evidence that “premature solidification” may take place if metal is poured with relatively low superheat into a cold mold cavity. Although this issue is of great importance to the solidification structure, it was not treated numerically in the existing literature. For this purpose, a 3-phase volume-averaging model is used to simulate the mold-filling process by considering the nucleation, the initial growth of globular equiaxed crystals, and the transport of the crystals. These calculated as-filled conditions obtained at different pouring temperatures replace the previously assumed initial conditions, which helps in improving the as-cast structure predictions. The predicted structures of various pouring temperatures are quantitatively and qualitatively compared with the experimental outcomes to evaluate the modeling results.

## II. MODEL FEATURES

The mold filling was simulated by using a 3-phase globular solidification model. A detailed description of the transport equations and the definitions of the corresponding source terms are provided in References 24–28. The main features and assumptions of the model are summarized as follows:

- The 3 phases are the air phase, the liquid metal, and the solidifying equiaxed globular crystals. They are quantified with the corresponding volume fractions  $f_a$ ,  $f_l$ , and  $f_e$ . They move with the corresponding velocities:  $\mathbf{u}_a$ ,  $\mathbf{u}_l$ , and  $\mathbf{u}_e$ .
- The morphology of equiaxed crystals is assumed as a sphere, and the formation of columnar crystal is ignored.
- A three-parameter heterogeneous nucleation law<sup>[29,30]</sup> is implemented to model the nucleation of the equiaxed crystals. The transport of the number density of the equiaxed crystals is calculated according to the solid velocity.
- The mass exchange between liquid and solid during the solidification of equiaxed crystals is determined by the diffusion-governed growth of the spherical crystal.
- The liquid–solid mass exchange introduces an additional source term for the momentum conservation equations of liquid and solid phases, but no mass or species exchange between air and the other phases.
- Grain sedimentation and thermosolutal convection are considered. Nevertheless, the forced convection associated with pouring is dominant.
- The remelting of the solid and the dissolution of the formed equiaxed nuclei are allowed. Superheating the solid and liquid mixture introduces two source terms: One for the remelting-induced mass transfer in the mass conservation equation, and one for the transport equation of the crystals. The rate of the remelting and the rate of the dissolution of nuclei are dependent on the superheat.

After the mold filling, a 5-phase mixed columnar-equiaxed solidification model with dendritic morphology<sup>[18–21]</sup> is applied to simulate the formation of the as-cast structure and the CET. The main features and assumptions of the 5-phase model are summarized as follows:

- The three hydrodynamic phases, denoted as e-, c-, and l-phases (Figure 1), are considered and quantified with their volume fractions,  $f_e$ ,  $f_c$ , and  $f_l$ . They move with the corresponding velocities:  $\mathbf{u}_e$ ,  $\mathbf{u}_c$  and

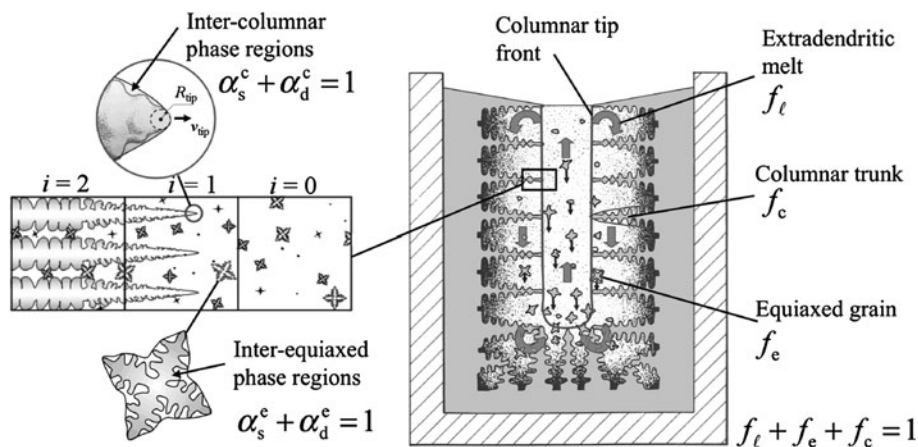


Fig. 1—Schematic of the mixed columnar-equiaxed solidification in an ingot casting.

- $\mathbf{u}_l$ . The columnar grain velocity  $\mathbf{u}_c$  is predefined as zero, whereas  $\mathbf{u}_e$  and  $\mathbf{u}_l$  are solved numerically. The air phase is not considered here.
- The dendritic growth of crystals is taken into consideration as shown in Figure 1. Two distinct phase regions exist within the crystal envelope: the solid dendrites and interdendritic melt. It is assumed that the interdendritic melt is transported with the solid dendrites and is generally enriched with the solute element to a larger extent than the extradendritic melt surrounding the crystals. Therefore, five “thermodynamic” phase regions are defined in the system: The solid dendrites and interdendritic melt in the equiaxed grain, the solid dendrites and interdendritic melt in the columnar dendrite trunk, and the extradendritic melt. Each region has corresponding volume fractions:  $f_s^e$ ,  $f_d^e$ ,  $f_d^c$ , and  $f_l$  and is characterized by its corresponding solute concentration:  $c_s^e$ ,  $c_d^e$ ,  $c_s^c$ ,  $c_d^c$ , and  $c_l$ . Inside an equiaxed grain, volume fractions of interdendritic liquid and solid dendrites are quantified, respectively, with  $\alpha_d^e$  and  $\alpha_s^e$ ; hence  $f_d^e = \alpha_d^e f_e$  and  $f_s^e = \alpha_s^e f_e$ . Inside a columnar dendrite trunk:  $f_d^c = \alpha_d^c f_c$  and  $f_s^c = \alpha_s^c f_c$ .
  - The same nucleation law, parameters, and equiaxed transport equation as the ones used for the 3-phase mold-filling model are used here. The growth of columnar trunks is assumed to start at the mold wall. The position of the columnar tip is tracked explicitly.<sup>[11,12]</sup>
  - The expansion of the grain envelope and the solidification of the interdendritic melt are treated differently. The expansion of the envelopes is determined by dendrite growth kinetics—using the Kurz–Giovanola–Trivedi model for the growth of columnar primary dendrite tips and the Lipton–Glicksman–Kurz model for the growth of columnar secondary dendrite tips (radial growth of the columnar trunk) and equiaxed primary dendrite tips. The solidification of the interdendritic melt is driven by the supersaturation of the interdendritic melt and governed by the diffusion in the interdendritic melt region.
  - Two columnar tip-blocking mechanisms are implemented to calculate the CET: One is the hard blocking,<sup>[6]</sup> and the other is the soft blocking.<sup>[9]</sup> The hard-blocking mechanism suggests that CET might occur when the equiaxed grains ahead of the columnar dendrite tip exceeds a critical volume fraction ( $f_{e,CET} = 0.49$ ). The soft-blocking mechanism suggests that the growth driving force (constitutional undercooling) is exhausted because of the enrichment with the solute element rejected by the growing equiaxed grains, which stops the growth of columnar primary dendrite tips. For both the 3- and the 5-phase models, the volume-averaging approach was employed to formulate the conservation equations of mass, momentum, species, and energy for the assigned phases. In addition to the grain transport equation, the former conservation equations were solved sequentially at each time step with implicit linearization based on the control volume method. The solidification models were implemented in an Eulerian multiphase CFD code (ANSYS Fluent 6.3.26).<sup>[31]</sup>

### III. SIMULATION SETUP

For the simulation of columnar/equiaxed solidification by means of the 5-phase model, a 2D axisymmetric grid was constructed (Figure 2) whereby the top surface profile is similar to that of the real casting. In order to simulate mold filling, this grid was additionally provided with one velocity inlet at the top for pouring the liquid alloy. The liquid alloy is poured at temperatures of 973 K, 1023 K, and 1073 K (700 °C, 750 °C, and 800 °C). The initial concentration of the poured melt was set at 4.0 wt pct and is assumed to carry  $1.0 \times 10^7 \text{ m}^{-3}$  of the heterogeneous nucleation sites. The parameters which are used for the nucleation model are based on experimental measurements by Ahmadein and co-workers.<sup>[32]</sup> From the casting experiments, the pouring speed was estimated to be 1.037 m/s for a corresponding filling time of ~5.5 seconds. A constant heat-transfer coefficient of  $120 \text{ W m}^{-2} \text{ K}^{-1}$  was provided at the outer walls of the mold and  $2900 \text{ W m}^{-2} \text{ K}^{-1}$  at the mold/melt interface. The mold was initially filled with air (with phase fraction,  $f_a \sim 1$ ) at the ambient temperature. During the process of pouring, air is allowed to escape from the top of the mold through a pressure outlet boundary condition. A fixed time-stepping scheme was employed with a time step between  $10^{-5}$  and  $10^{-4}$  seconds.

To calculate the subsequent ingot solidification after mold filling, the same ingot and mold grid were used after excluding the pouring inlet and air outlet. The average temperature,  $f_l$ ,  $f_e$ ,  $n$ ,  $c_l$ , and  $c_e$  of the as-filled ingot are used to initialize the solution of ingot solidification using the 5-phase mixed columnar-equiaxed model. The same ingot and mold grid are used. The heat-transfer coefficient at the outer wall remains unchanged, whereas it was reduced at the melt/mold

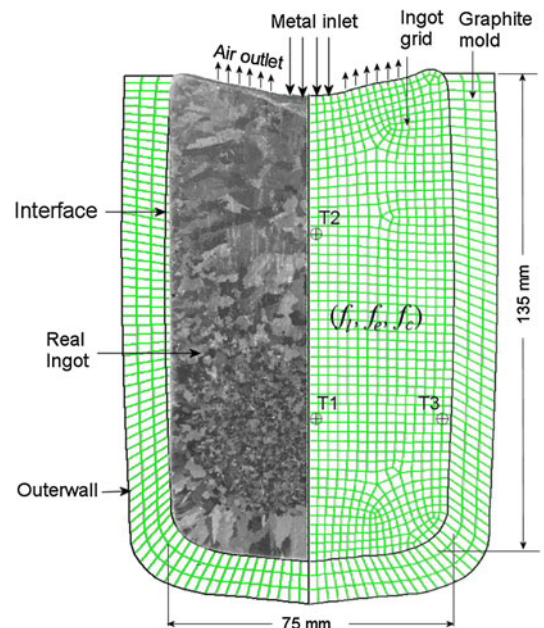


Fig. 2—Simulation grid of ingot and mold.

interface to 1000 and 125 W m<sup>-2</sup> K<sup>-1</sup> above and below the liquidus temperature, respectively. The initial  $f_l$  and  $f_e$  are provided from the 3-phase mold-filling simulation, whereas  $f_c$  is assumed to be 10<sup>-5</sup>. The columnar primary dendrites were initialized with tips located at the mold/melt interface cells. An adaptive time-stepping scheme was employed with a minimum time step of 10<sup>-4</sup> seconds. The grid was equipped with some control points and thermocouples, *e.g.*, T1, T2, and T3. Further modeling parameters and the thermophysical data are listed in Table I.

#### IV. EXPERIMENT

The Al-4.0 wt pct Cu alloy was melted and poured into a clay-bonded graphite crucible at different pouring temperatures, namely 973 K, 1023 K, and 1073 K

(700 °C, 750 °C, and 800 °C). Crucibles were initially set at the room temperature. Mold filling is accomplished in ~5.3 seconds with an average pouring velocity of 1.037 m/s. After pouring, the top was covered, and they were let to cool down in the normal atmosphere. After solidification, specimens were cut, ground, polished, and etched for macroscopic examination. The resulting macrographs are shown in Figure 3.

The as-cast structures of various samples are shown in Figure 3. It is obvious from a first glance that a lower pouring temperature favors the formation of equiaxed grains. In addition, the equiaxed grain size is reduced when the pouring temperature decreases. Concerning the ingot poured at 1073 K (800 °C) (Figure 3(a)), the core of the ingot (region A) is mainly equiaxed with finer grains near the bottom and with coarser grains at the top. These equiaxed grains are mixed with the columnar ones at the region boundaries. In the outer region

Table I. Simulation Parameters for Al-4.0 Weight Percentage Cu Alloy

Thermophysical data	Nucleation parameters
Solute concentration of raw material = 4.0 wt pct Cu	$n_{\max} = 1.48 \times 10^{11} \text{ m}^{-3}$
Eutectic concentration = 33.2 wt pct Cu	$\Delta T_N = 28.84 \text{ K}$
Eutectic temperature = 821.35 K	$\Delta T_\sigma = 0.17 \text{ K}$
Liquidus slope = -260 K/wt pct	$n_0 = 10^7$ (for 3-phase simulation)
Partition coefficient = 0.145	Morphological parameters
Latent heat of fusion = 389.32 kJ/kg	$\Phi_{\text{env}}^c = 0.48$
Thermal capacity = 1100 J/kg K	$\Phi_{\text{sph}}^c = 0.4$
Thermal conductivity of liquid = 87 W/m K	$\Phi_{\text{env}}^e = 0.80$
Thermal conductivity of solid = 180 W/m K	$\Phi_{\text{sph}}^e = 0.5$
Diffusion coefficient in liquid = $5.0 \times 10^{-9} \text{ m}^2/\text{s}$	Primary dendrite arm spacing = 500 $\mu\text{m}$
Diffusion coefficient in solid = $8.0 \times 10^{-13} \text{ m}^2/\text{s}$	Secondary dendrite arm spacing = 100 $\mu\text{m}$
Liquid viscosity = 0.0012769 kg/m s	
Thermal expansion coefficient = 0.0001 K <sup>-1</sup>	
Solutal expansion coefficient = -0.92 wt pct <sup>-1</sup>	

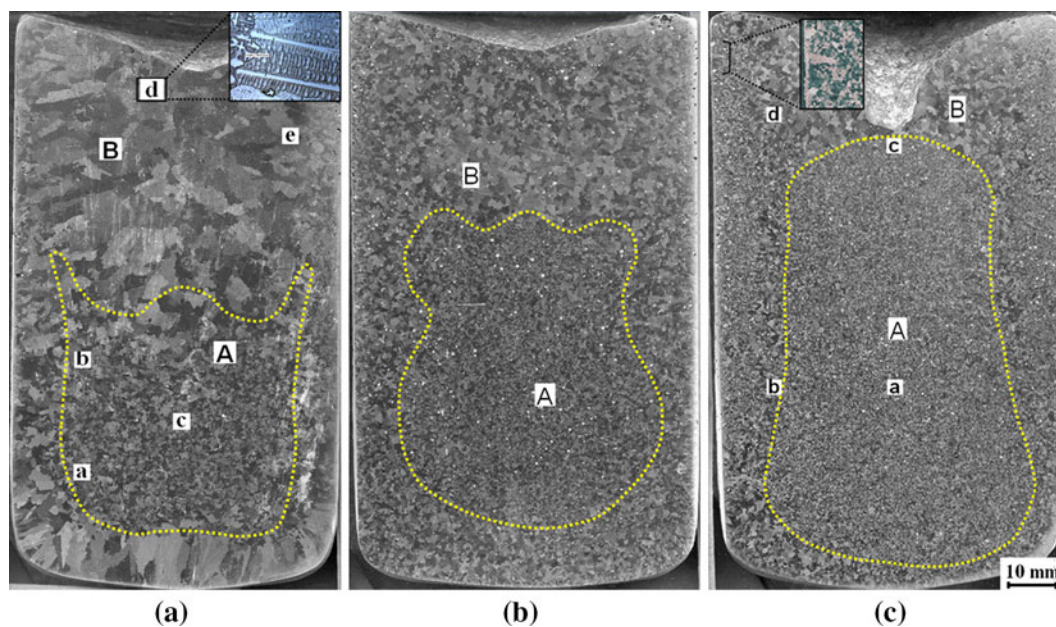


Fig. 3—The as-cast structure of Al-4 pct Cu ingots poured at (a) 1073 K (800 °C), (b) 1023 K (750 °C), and (c) 973 K (700 °C). Capital letters denote macroscopic regions; small letters denote microstructure characterization points.

(region B), it is evident that the columnar trunks grow perpendicular to the mold walls. The structure of the ingot poured at 1023 K (750 °C) (Figure 3(b)) is mainly very fine equiaxed in the core (region A) and relatively coarse equiaxed in the exterior (region B) which may interfere with some columnar grains which grow from the wall. A further reduction of the pouring temperature (Figure 3(c)) results in very fine equiaxed grains at the ingot core (region A) with a fine-grained exterior. The top (region B) features coarser equiaxed grains, mixed with a few columnar grains coming from the mold wall.

## V. SIMULATION RESULTS

The 3-phase model was used to simulate the mold filling of ingots poured at two extreme pouring temperatures: 1073 K and 973 K (800 °C and 700 °C). The calculated temperature after a filling time of 5 seconds for the ingot poured at 973 K (700 °C) (Figure 4(a)) showed that the superheated metal jet retains its temperature until it bumps up against the mold base. Thus, it exchanges its heat with the cold mold, cools down, and continues to cool, while it is streaming upward, close to the mold wall. Additional heat losses occur through the melt/air interface at the top. As a result, the top of the ingot is colder than the core and the bottom. Owing to the effect of the melt convection, a relatively high solid fraction (Figure 4(b)) is formed within the mixture vortex compared with its core which retains a relatively higher temperature. In addition, the nucleation and the crystal growth rates are much higher at the top than the rest region of the ingot (Figures 4(c) and (d)). The formed grains are redistributed in response to the convective stream. Some of them survive, while some are remelted at the hotter regions. Thus, the vortex center exhibits low  $n$ . The falling hot metal jet maintains

the minimum  $f_e = 10^{-5}$  and  $n = 10^7 \text{ m}^{-3}$  and  $d_e = 1 \mu\text{m}$  (assumed as inlet boundary condition).

The average value of  $f_e$  and  $n$  over the melt-filled domain are monitored during mold filling and plotted versus the pouring time, as shown in Figure 5. For the ingot poured at 973 K (700 °C), equiaxed grains nucleate very early at  $\sim 0.2$  seconds and a very high number density ( $\sim 1.0 \times 10^{10} \text{ m}^{-3}$ ) is formed when the liquid metal touches the cold bottom of the mold. Afterward,  $n$  fluctuates and gradually decreases. After 1.5 seconds,  $n$  increases tremendously to reach a steady-state value of about  $1.1 \times 10^{10} \text{ m}^{-3}$  after 4.0 seconds. In the same case, the volume fraction of the solid behaves similar to  $n$  and reaches about 0.055 after the filling of the mold. On the other hand, the nucleation is delayed for the highly superheated ingot [1073 K (800 °C)] to start at  $\sim 0.45$  seconds with a lower grain production rate. The

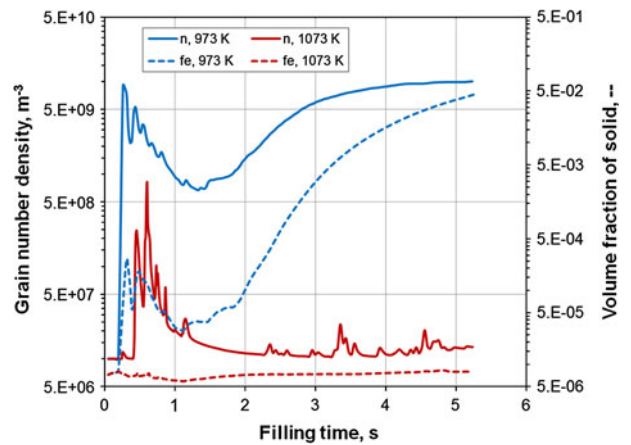


Fig. 5—Evolution of the average of  $n$  and  $f_e$  during the mold-filling process at 973 K and 1073 K (700 °C and 800 °C) pouring temperature.

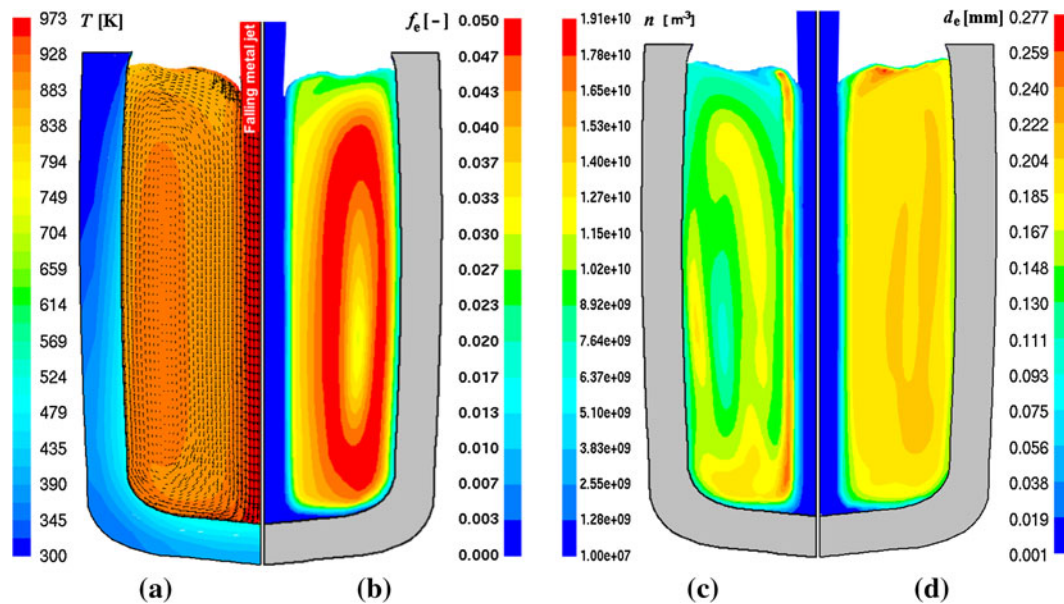


Fig. 4—Calculated results for the ingots poured at 973 K (700 °C) after a filling time of 5 s: (a) temperature field with superimposed solid velocity vectors, (b)  $f_e$ , (c)  $n$ , and (d) grain diameter of the solid.

peak value ( $\sim 6.0 \times 10^8 \text{ m}^{-3}$ ) decreases progressively as the pouring of the hot melt proceeds. The grain growth is negligible, since the initial  $f_e$  is maintained. The as-filled mold contains an average of  $n \sim 1.3 \times 10^7 \text{ m}^{-3}$  and  $f_e \sim 0.0$ , *i.e.*, similar to the initial melt state.

The calculated results of the as-filled state are used as initial conditions for the subsequent solidification calculation using the 5-phase mixed columnar-equiaxed model. The resulting cooling curves at the thermocouple point T1 (positions shown in Figure 2) are plotted versus those of the experiments as shown in Figure 6. The calculated cooling rates and the total solidification time are nearly similar to those of the experiments. The solidification plateau at the liquidus temperature is reproduced by the simulation. The predicted as-cast structure of the ingot poured at 1073 K (800 °C) is shown in Figure 7. Two zones could be easily distinguished in the as-cast structure of the equiaxed phase

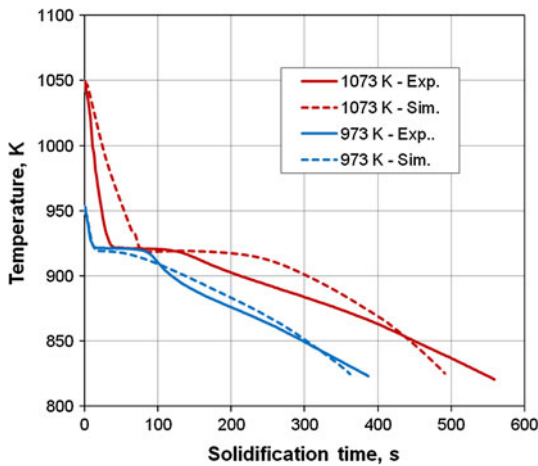


Fig. 6—Measured and calculated cooling curves of the ingots poured at 973 K and 1073 K (700 °C and 800 °C).

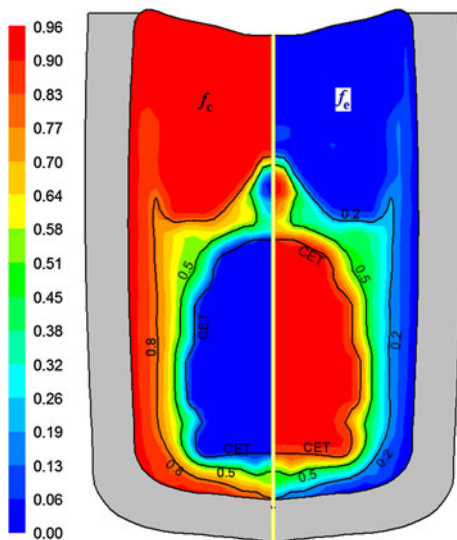


Fig. 7—Calculated volume fractions of the columnar and equiaxed phases of the ingot poured at 1073 K (800 °C).

region at the ingot core and the columnar phase region in the exterior. Both regions are separated by a mixed columnar-equiaxed zone. The final position of the columnar primary dendrite tips is indicated by the CET-line. The equiaxed zone is vertically extended in the mold near the sidewall with a lower volume fraction. At a horizontal section 40 mm above the bottom, the calculated volume fraction of the phases was plotted versus the ingot radius along with the real-to-scale as-cast structure, as demonstrated in Figure 8. The predictions of the  $f_e$  and  $f_c$  finely match the macrograph of the same region. A fully equiaxed structure can be noticed on the left of the CET-line, whereas  $f_c$  increases tremendously on the right of the CET-line. A mixed structure between 18 and 29 mm can be discerned. An overall eutectic volume fraction of 9 pct was formed.

In addition to the above results, the model provided other results such as the grain number density and the solute concentration in each phase. The calculated diameter of the equiaxed grains and the columnar trunks are shown in Figure 9. The finest equiaxed grains and the coarsest columnar trunks exist at the exterior of the ingot and vice versa inside the CET-line.

Analogous to the real as-cast structure (Figure 3(a)), the calculated structure has relatively fine equiaxed grains close to the bottom of “region-A” and coarse grains at the top of the same region. At the horns of “region-A,” the size of equiaxed grains gradually decreases toward the top. Very tiny equiaxed grains (400- $\mu\text{m}$  diameter with  $f_e \sim 5$  pct) may coexist along with columnar grains at the ingot top and peripherals. Compared with the ingot peripherals, very coarse columnar trunks are obtained at the top of “region-B.”

The predicted as-cast structure of the ingot poured at 973 K (700 °C) is shown in Figure 10. The structure is almost equiaxed, except for the corners that contain a tiny amount of columnar grains. The complementary volume fraction to  $f_e$  inside the CET-line represents the formed eutectic. A very high number density for the equiaxed grains is formed at the ingot core. A lower

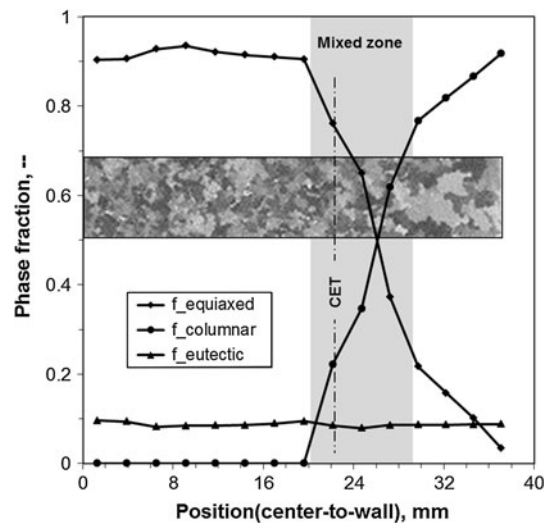


Fig. 8—Phase fraction distribution from center-to-wall at a line 40 mm above the bottom.

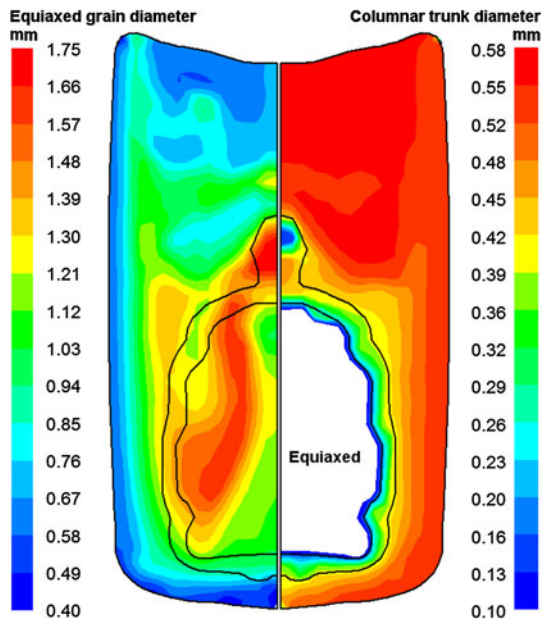


Fig. 9—Calculated diameters of equiaxed grains and the columnar trunks for the sample poured at 1073 K (800 °C).

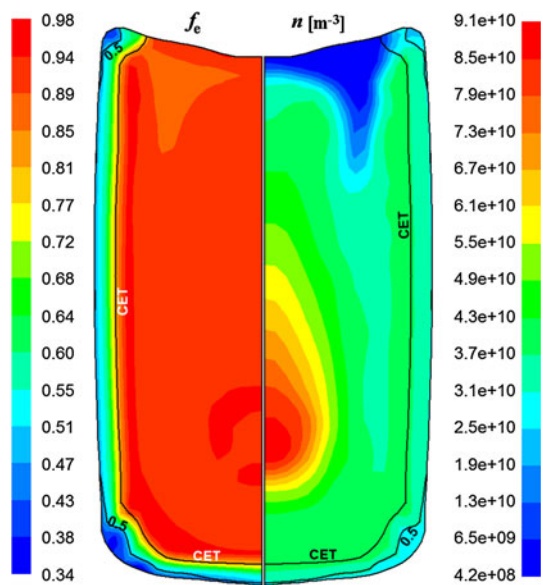


Fig. 10—Calculated  $f_e$ ,  $n$ , and CET of the ingot poured at 973 K (700 °C) using the predicted initial conditions.

number density is formed at ingot exterior and the minimum, which corresponds to the coarser grains and exists at the top of the ingot.

## VI. MODEL EVALUATION AND DISCUSSION

During mold filling, the assumption for the model that the equiaxed growth of grains is globular seems very reasonable. It is well established that the formation of columnar grains starts with nuclei sticking to the mold walls. During the process of mold filling, the

continual pouring and splashing of superheated melt eliminates any chance for grains to stick to the walls. After the mold filling, convection and agitation are reduced substantially, and the conditions may favor the columnar growth. In this case, switching to the 5-phase model is more convenient to consider the columnar/equiaxed dendritic growth in a competitive manner.

The results of  $n$  (Figure 5) exhibit a delayed nucleation for the casting poured at 1073 K (800 °C) compared with that poured at 973 K (700 °C). The reason for this is the additional time needed to undercool the melt and dissipate the extra superheat. According to the nucleation model, at the moment when the hot metal bumps against the mold bottom, the nucleation rate for the melt poured at 973 K (700 °C) is much higher compared with that for the melt poured at 1073 K (800 °C). In fact, these results support the nucleation theory known as the “big-bang.”<sup>[2]</sup> The formed nuclei may survive or remelt depending on the pouring conditions, *e.g.*, after the first bump of the metal jet against the mold bottom, and, owing to the continual pouring of the hot melt, the nucleation rate decreases. The reason for this lies in the remelting and the reduced cooling rate. After about 1.5 seconds,  $n$  increases progressively for the low superheated [973 K (700 °C)] melt, whereas the initially formed big-bang crystals of a highly superheated one [1073 K (800 °C)] remelt gradually and reach a state that is very close to the original state of the incoming melt at the inlet. The average volume fraction of the solid reaches as high as  $\sim 0.055$  for the casting poured at 973 K (700 °C), while it remains the same as the initial melt state ( $f_e = \sim 0.0$ ) for the casting poured at 1073 K (800 °C).

In previous studies,<sup>[22,23]</sup> the simulation of mold filling was ignored and replaced by assuming a higher  $n_0$  for the ingot poured at a low temperature. The results of a parameter study based on this assumption reveal the impact of  $n_0$  (varying from  $10^7$  to  $10^9$   $m^{-3}$ ) on the CET, where the equiaxed region expands when  $n_0$  increases. Nevertheless, the modification of  $n_0$  alone is insufficient to suppress the growth of the columnar grains for the ingot poured at a lower temperature, and this assumption failed to reproduce an as-cast structure similar to that shown in Figure 3(c). The current two-stage simulation strategy showed that not only does the initial  $n_0$  have to be considered depending on the pouring temperature, but also all the other solidification quantities, in particular  $f_e$ . The CET criterion is based on the competitive growth between the columnar and equiaxed phases. A simulation which ignores the impact of mold filling on the initial  $f_e$  allows the columnar grains with tips initialized at the mold interface to win this competition even at a low pouring temperature, which results in false predictions. After adopting the new strategy, the equiaxed grains initially have the majority ( $n_0 = 1.1 \times 10^{10} m^{-3}$  and  $f_e = 0.055$ ) for the ingot poured at 973 K (700 °C). Therefore, the equiaxed phase could survive and limit the growth of the columnar phase, which would lead to an improved prediction (Figures 3(c) and 10).

The above results, based on the new two-stage modeling strategy, exhibit a good qualitative agreement regarding the phase distribution, grain size, and CET. The numer-

Table II Measured and Calculated Microstructural Quantities at Selected Points

$T_{\text{Pouring}}$ [K (°C)]	Quantity Point*	$n_c$ (m <sup>-3</sup> )				$d_c$ (mm)	
		a	b	c	d	d	e
1073 (800)	measured	$2.9 \times 10^9$	$7.0 \times 10^8$	$2.8 \times 10^9$	—	0.73	0.65
	calculated	$1.1 \times 10^9$	$6.2 \times 10^8$	$1.3 \times 10^9$	—	0.553	0.54
973 (700)	measured	$5.4 \times 10^{10}$	$2.8 \times 10^{10}$	$1.8 \times 10^{10}$	$2.5 \times 10^9$	—	—
	calculated	$6.9 \times 10^{10}$	$3.2 \times 10^{10}$	$2.4 \times 10^{10}$	$6.0 \times 10^9$	—	—

\*The points a, b, c, etc. correspond to the positions as marked in Figs. 3(a) and (c).

ically predicted as-cast structure of the 1073 K (800 °C) ingot (Figure 7) features an equiaxed core and a columnar exterior similar to experiment (Figure 3(a)). The real as-cast structure contains coarse equiaxed and columnar trunks at the top of the regions “A” and “B,” respectively, which is already predicted in Figure 7. The qualitative comparison of the results of the ingot poured at 973 K (700 °C) (Figures 3(c) and 10) exhibit a good agreement. A fully equiaxed structure with a fine core and a coarse top is predicted similar to the experiment. Some columnar grains could be distinguished at the mold corners by analogy with the real structure. As further evidence, a quantitative comparison of the grain number density “ $n_c$ ,” with trunk diameter “ $d_c$ ” at selected points (a through e in Figure 3(a)) is summarized in Table II.

The final findings seem very promising and emphasize the significance of modeling the process of mold filling. Further numerical and experimental mold-filling verifications will be suggested in the forthcoming study. In addition, the impact on the as-cast structure has to be studied as well. At this point, an additional message may be addressed to the commercial software developers, namely that they should pay a greater attention to the probable premature nucleation and solidification during the mold filling in casting processes.

## VII. CONCLUSIONS

The 3-phase mold-filling simulations revealed the impact of pouring temperature on the premature equiaxed solidification for the as-filled state of the ingot. Premature solidification and the “big-bang” nucleation are numerically observed during the pouring of low superheated melt. Considering the “big-bang” nucleation and the premature solidification during the mold-filling process as initial conditions, the subsequent as-cast structure predictions using the 5-phase mixed columnar-equiaxed solidification model can be improved significantly. A good quantitative agreement with the real as-cast structure (Al-4.0 wt pct Cu) poured at 973 K and 1073 K (700 °C and 800 °C) was achieved. The current study raises an important issue for future model development. Greater attention should be paid to the nucleation and the premature solidification that occurs during the mold-filling process. Further numerical and experimental mold-filling verifications are going to be our objectives for the future studies.

## ACKNOWLEDGMENTS

This study was financially supported by the FWF Austrian Science Fund (P23155-N24). The casting experiments were performed by Georg Nunner and Gerhard Hochleithner.

## REFERENCES

1. G. Form and J. Wallace: *Mod. Cast.*, 1960, vol. 37, pp. 144–53.
2. B. Chalmers: *Principles of Solidification*, John Wiley & Sons, New York, 1964.
3. M. Flemings: *Solidification Processing*, McGraw-Hill, New York, 1974.
4. A. Ohno: *Solidification: The Separation Theory and Its Practical Applications*, Springer-Verlag, Berlin, 1987.
5. R. Morando, H. Biloni, G. Cole, and G. Bolling: *Metall. Trans.*, 1970, vol. 1, pp. 1407–12.
6. J. Hunt: *Mater. Sci. Eng.*, 1984, vol. 65, pp. 75–83.
7. M. Gäumann, R. Trivedi, and W. Kurz: *Mater. Sci. Eng. A*, 1997, vols. 226–228, pp. 763–69.
8. C. Wang and C. Beckermann: *Metall. Mater. Trans. A*, 1994, vol. 25A, pp. 1081–93.
9. M. Martorano, C. Beckermann, and Ch.-A. Gandin: *Metall. Mater. Trans. A*, 2003, vol. 34A, pp. 1657–74.
10. M. Martorano and V. Biscuola: *Acta Mater.*, 2009, vol. 57, pp. 607–15.
11. M. Wu and A. Ludwig: *Metall. Mater. Trans. A*, 2006, vol. 37A, pp. 1613–31.
12. M. Wu and A. Ludwig: *Metall. Mater. Trans. A*, 2007, vol. 38A, pp. 1465–75.
13. Ch.-A. Gandin: *Acta Mater.*, 2000, vol. 48, pp. 2483–2501.
14. Ch.-A. Gandin: *ISIJ Int.*, 2000, vol. 40, pp. 971–79.
15. A. McFadden, D. Browne, and Ch.-A. Gandin: *Metall. Mater. Trans. A*, 2009, vol. 40A, pp. 662–72.
16. A. McFadden and D. Browne: *Appl. Math. Model.*, 2009, vol. 33, pp. 1397–1416.
17. C. Siqueira, N. Cheung, and A. Garcia: *Metall. Mater. Trans. A*, 2002, vol. 33A, pp. 2107–18.
18. M. Wu and A. Ludwig: *Acta Mater.*, 2009, vol. 57, pp. 5621–31.
19. M. Wu and A. Ludwig: *Acta Mater.*, 2009, vol. 57, pp. 5632–44.
20. M. Wu, A. Fjeld, and A. Ludwig: *Comput. Mater. Sci.*, 2010, vol. 50, pp. 32–42.
21. M. Wu, A. Ludwig, and A. Fjeld: *Comput. Mater. Sci.*, 2010, vol. 50, pp. 43–58.
22. M. Wu, G. Nunner, A. Ludwig, J.H. Li, and P. Schumacher: *3rd Int. Conf. on Advances in Solidification Processes*, Aachen, Germany, IOP Conf. Series: Mater. Sci. Eng., 2011, vol. 27.
23. M. Wu, M. Ahmadein, A. Kharicha, A. Ludwig, J.H. Li, and P. Schumacher: *13th MCWASP*, Schladming, Austria, IOP Conf. Ser.: Mater. Sci. Eng., 2012, vol. 33.
24. A. Ludwig and M. Wu: *Metall. Mater. Trans. A*, 2002, vol. 33A, pp. 3673–83.
25. T. Wang, S. Yao, X. Zhang, J. Jin, M. Wu, A. Ludwig, B. Pustal, and A. Bührig-Polaczek: *Acta Metall. Sinica*, 2006, vol. 42, pp. 584–90.
26. T. Wang, T. Li, Z. Cao, J. Jin, T. Grimming, A. Bührig-Polaczek, M. Wu, and A. Ludwig: *Acta Metall. Sinica*, 2006, vol. 42, pp. 591–98.

27. M. Ahmadein: "Experimentation and Modeling of Grain Nucleation and Solidification of Aluminum Alloys in Absence and Presence of Shear," Ph.D., Foundry Institute at RWTH-Aachen University, Germany, Shakerverlag, 2009.
28. M. Wu, A. Ludwig, and J. Luo: *Mater. Sci. Forum*, 2005, vols. 475–479, pp. 2725–30.
29. Ph. Thevoz and M. Rappaz: *Metall. Trans.*, 1989, vol. 20A, pp. 311–22.
30. M. Rappaz and Ch.-A. Gandin: *Acta Metall. Mater.*, 1993, vol. 41, pp. 345–60.
31. *FLUENT 6.3 User's Guide*, FLUENT Inc., Lebanon, NH, 2006, pp. 537–43.
32. M. Ahmadein, B. Pustal, R. Berger, E. Subasic, and A. Bührig-Polaczek: *Metall. Mater. Trans. A*, 2009, vol. 40A, pp. 646–53.